Primitive Helium Is Sourced From Seismically Slow Regions in the Lowermost Mantle

C. D. Williams, S. Mukhopadhyay, M. L. Rudolph, B. Romanowicz

AGU100 ADVANCING EARTH AND SPACE SCIENCE

Geochemistry, Geophysics, Geosystems

RESEARCH ARTICLE
10.1029/2019GC008437

Key Points:
- Geodynamic models predict the lateral offset of plume source locations in the lower mantle from their present-day surface expressions
- These models predict a strong relationship between primitive (low) $^{4}He/^{3}He$ ratios and seismically slow regions of the lower mantle
- These models predict no significant relationship between recycled, high $^{208}Pb^{*}/^{206}Pb^{*}$ ratios, and seismically slow regions of the lower mantle

Supporting Information:
- Supporting Information S1
- Figure S1
- Figure S2
- Figure S3
- Table S1

Correspondence to:
C. D. Williams,
cdwill@ucdavis.edu

Citation:
Williams, C. D., Mukhopadhyay, S., Rudolph, M. L., & Romanowicz, B. (2019). Primitive helium is sourced from seismically slow regions in the lowermost mantle. *Geochemistry, Geophysics, Geosystems*, *20*, 4130–4145. https://doi.org/10.1029/2019GC008437

Received 9 MAY 2019
Accepted 26 JUL 2019
Accepted article online 31 JUL 2019
Published online 19 AUG 2019

Primitive Helium Is Sourced From Seismically Slow Regions in the Lowermost Mantle

C. D. Williams[1], S. Mukhopadhyay[1], M. L. Rudolph[1], and B. Romanowicz[2,3,4]

[1]Department of Earth and Planetary Sciences, University of California at Davis, Davis, CA, USA, [2]Department of Earth and Planetary Science, Berkeley Seismological Laboratory, University of California at Berkeley, Berkeley, CA, USA, [3]Collège de France, Paris, France, [4]Institut de Physique du Globe de Paris, Paris, France

Abstract A major goal in Earth Science has been to understand how geochemical characteristics of lavas at the Earth's surface relate to the location and formation history of specific regions in the Earth's interior. For example, some of the strongest evidence for the preservation of primitive material comes from low $^{4}He/^{3}He$ ratios in ocean island basalts, but the location of the primitive helium reservoir(s) remains unknown. Here we combine whole-mantle seismic tomography, simulations of mantle flow, and a global compilation of new and existing measurements of the $^{4}He/^{3}He$ ratios in ocean island basalts to constrain the source location of primitive $^{4}He/^{3}He$ material. Our geodynamic simulations predict the present-day surface expression of plumes to be laterally offset from their lower mantle source locations. When this lateral offset is accounted for, a strong relationship emerges between minimum $^{4}He/^{3}He$ ratios in oceanic basalts and seismically slow regions, which are generally located within the two large low shear-wave velocity provinces (LLSVPs). Conversely, no significant relationship is observed between maximum $^{208}Pb^{*}/^{206}Pb^{*}$ ratios and seismically slow regions in the lowermost mantle. These results indicate that primitive materials are geographically restricted to LLSVPs, while recycled materials are more broadly distributed across the lower mantle. The primitive nature of the LLSVPs indicates these regions are not composed entirely of recycled slabs, while complementary xenon and tungsten isotopic anomalies require the primitive portion of the LLSVPs to have formed during Earth's accretion, survived the Moon-forming giant impact, and remained relatively unmixed during the subsequent 4.5 billion years of mantle convection.

Plain Language Summary Geochemical variations in volcanic rocks erupted at Earth's surface indicate differences in mantle composition, but our understanding of the location, formation, and history of compositionally distinct mantle domains remains incomplete. In particular, some hotspot lavas contain signatures of primitive regions within the mantle that have remained relatively isolated and unprocessed throughout Earth's history. Here we use models of mantle flow to predict the locations within the mantle that are sampled by the mantle plumes associated with hotspot volcanism. Combining these models of mantle flow with state-of-the-art seismic images and a comprehensive catalog of hotspot lava geochemistry, we find that hotspots with a more primitive geochemical signature (as indicated by the isotopes of helium) sample the two large low shear-velocity provinces in the lowermost mantle. Complementary constraints from xenon and tungsten isotope ratios associated with primitive materials then require these continent-sized provinces in Earth's deep interior formed early in Earth's history, survived the violent Moon-forming giant impact, and remained relatively unmixed with the rest of the solid Earth over the past 4.5 billion years.

1. Introduction

The geochemistry of basalts erupted at mid-ocean ridges and ocean islands provides critical evidence for preservation of primitive regions of the mantle that have escaped significant processing over 4.5 billion years of Earth history (e.g., Mukhopadhyay, 2012; Mundl et al., 2017). The distribution of these primitive regions within the mantle places first-order constraints on models of mantle convection (Tackley, 2000). Some of the strongest evidence for the preservation of primitive material comes from low $^{4}He/^{3}He$ ratios in ocean island basalts (OIBs; Graham et al., 2016, 2014, 1996, 1992; Kurz, 1982; Moreira, 2013). However, our understanding of the location, formation, and history of these primitive mantle domains remains incomplete.

Helium behaves as an extremely incompatible element during mantle melting (Graham et al., 2016) and unlike lithophile elements is not recycled back into the mantle, which makes it a unique tracer of

primitive regions of the mantle (Graham et al., 2016, 2014, 1996, 1992; Kurz, 1982; Moreira, 2013). Helium has two naturally occurring isotopes. Helium-3 in the mantle is primordial in origin, while nearly all helium-4 has been produced through the radioactive decay of ^{238}U, ^{235}U, and ^{232}Th through geological time. Therefore, the $^4He/^3He$ ratio is a function of the time-integrated $(U+Th)/^3He$ ratio. Mid-ocean ridge basalts (MORBs) removed from plume influences (characterized by, e.g., distance from nearest hotspot, topographic highs, and uniqueness of complementary trace element signatures; Graham, 2002; Moreira, 2013) display a narrow range of $^4He/^3He$ ratios approximately 80,000–100,000 (~7–9 R_A, where R_A is the atmospheric $^3He/^4He$ ratio; Graham et al., 1992, 1996, 2014; Kurz, 1982), reflecting high time-integrated $(U+Th)/^3He$ ratios in the MORB source. The high time-integrated $(U+Th)/^3He$ ratios suggest that the upper mantle has been depleted in incompatible elements due to repeated episodes of melt extraction associated with crust formation. On the other hand, many OIBs are characterized by both a larger range in $^4He/^3He$ ratios and more primitive values, with $^4He/^3He$ ratios reaching values as low as 14,200 (50 R_A) (Farley et al., 1992; Harðardóttir et al., 2017; Hilton et al., 1999; Jackson et al., 2008, 2009; Kurz et al., 2009, 1983; Kurz & Geist, 1999; Péron et al., 2016, 2017; Starkey et al., 2009; Stuart et al., 2003; Valbracht et al., 1997). These relatively low (primitive) $^4He/^3He$ ratios reflect low time-integrated $(U+Th)/^3He$ ratios, suggesting that some OIBs sample primitive regions of the mantle that have been less processed by melt extraction and/or addition of recycled materials.

Numerous models have been proposed for the location of the primitive helium. Early models interpreted primitive (low) $^4He/^3He$ ratios to reflect plumes sampling a less processed primitive lower mantle (below 660-km depth), while MORBs sample a relatively more processed upper mantle (Allègre et al., 1983). However, placing the boundary between a less processed lower mantle and more processed upper mantle at 660-km depth is at odds with tomographic images of slabs descending through the 660-km discontinuity (Fukao et al., 2001; Grand et al., 1997; Van Der Hilst et al., 1997). To satisfy seismic observations, including radial changes in the relative variations of bulk sound with shear wave velocities (Van Der Hilst & Karason, 1999), a global boundary between a less processed lower mantle and more processed upper mantle was placed at 1,600-km depth, and it was suggested that the lower mantle must be denser than the upper mantle in order to remain convectively isolated over long periods of geologic history (Kellogg et al., 1999). Rather than forming a global layer, it has recently been proposed that the primitive, low $^4He/^3He$ materials may be confined to discrete, compositionally distinct regions of the lowermost mantle (Deschamps et al., 2011).

Several lines of evidence suggest that the two large low-shear velocity provinces (LLSVPs; Woodhouse & Dziewonski, 1989) may be compositionally distinct from their surroundings. First, the anticorrelation between bulk and shear sound speed in the lowermost mantle is incompatible with shear-wave velocity variations arising solely from changes in temperature (Su & Dziewonski, 1997; Masters et al., 2000). Second, detailed waveform modeling studies require very sharp boundaries that may be incompatible with a purely thermal origin (He & Wen, 2009; Ni et al., 2002; To et al., 2005; Wang & Wen, 2007). Tidal tomography (Lau et al., 2017) as well as inversion of seismic data with constraints from gravity and other geophysical observables also points to the presence of chemically distinct material with higher than average density within the LLSVPs at the vary base of the mantle (e.g., Simmons et al., 2010). The presence of chemically distinct material within the LLSVPs, however, remains controversial, as other authors suggest the LLSVPs may be lighter than the ambient mantle (e.g., Koelemeijer et al., 2017). These conflicting results may eventually be reconciled if the different depth sensitivities of the respective data are considered (Romanowicz, 2017). The chemically distinct nature of the LLSVPs may promote their long-term stability, while small amounts of LLSVP material could be entrained and transported to the surface by mantle plumes (Deschamps et al., 2011). However, there is currently no direct evidence linking primitive $^4He/^3He$ materials to the LLSVPs.

Alternatively, the LLSVPs could be produced through the accumulation of subducted oceanic crust (Tackley, 2011; Tan & Gurnis, 2005). Lead isotope variations may allow us to identify the presence of oceanic crust in OIBs. Radiogenic lead isotopes (e.g., ^{208}Pb and ^{206}Pb) are the product of three distinct decay chains. The $^{207}Pb/^{204}Pb$ and $^{206}Pb/^{204}Pb$ ratios are a function of the time-integrated U/Pb ratio, while the $^{208}Pb/^{204}Pb$ ratio is a function of the time-integrated Th/Pb ratio. The lead isotope system can also provide information about the time-integrated Th/U ratio through the following equation:

$$\frac{^{208}Pb^*}{^{206}Pb^*} = \frac{^{208}Pb/_{^{204}Pb} - \left(^{208}Pb/_{^{204}Pb}\right)_i}{^{206}Pb/_{^{204}Pb} - \left(^{206}Pb/_{^{204}Pb}\right)_i}$$

where the asterisks denote the radiogenic component and the subscript i denotes the initial ratio [$(^{208}Pb/^{204}Pb)_i = 29.475$ and $(^{206}Pb/^{204}Pb)_i = 9.307$]. Therefore, the $^{208}Pb^*/^{206}Pb^*$ ratio measures the time-integrated ingrowth of the radiogenic ^{208}Pb and ^{206}Pb since the formation of the Earth. Uranium, thorium, and lead all behave as incompatible elements during mantle melting. Therefore, maximum $^{208}Pb^*/^{206}Pb^*$ ratios measured in OIBs reflect enriched materials such as oceanic crust that has been recycled back into the Earth's mantle. Ocean islands with the highest $^{208}Pb^*/^{206}Pb^*$ appear to be spatially correlated with the edges of the LLSVPs when projected radially into the mantle, indicating that the LLSVPs may be composed of geochemically enriched, recycled oceanic crust that has accumulated at the base of the mantle (Castillo, 1988; Harpp et al., 2014; Harrison et al., 2017; Hoernle et al., 2015; Huang et al., 2011; Payne et al., 2013; Weis et al., 2011). However, the practice of radially projecting surface observations into the deep mantle (Castillo, 1988; Harpp et al., 2014; Harrison et al., 2017; Hoernle et al., 2015; Huang et al., 2011; Jackson et al., 2018a, 2018b, 2017; Payne et al., 2013; Weis et al., 2011) is not physically justifiable if surface volcanism is laterally offset from its deep mantle source.

Seismic observations indicate that plumes are not strictly vertical features stretching from the core-mantle boundary to the surface (Bozdağ et al., 2016; French & Romanowicz, 2015; Montelli et al., 2006; Nelson & Grand, 2018; Rickers et al., 2013; Wolfe et al., 2009). Rather, many plume conduits are deflected laterally as they ascend into the upper mantle. As a consequence, the deep mantle roots of these conduits are frequently offset laterally with respect to the corresponding hotspots. However, seismic tomography does not adequately resolve all mantle plumes. Therefore, tracing the geochemistry of individual ocean islands from the surface to their source location in the lower mantle requires additional information from mantle flow models (e.g., Boschi et al., 2007; Konrad et al., 2018; Steinberger & Antretter, 2006; Steinberger et al., 2004).

In this paper, simulations of mantle flow are used to predict the offset of plume base locations from their surface expressions. Given these predictions, and assuming that all plumes originate from the lowermost mantle, the surface geochemistry of individual ocean island tracks is traced to their source location in the lower mantle. We then analyze the relationship between the geochemistry and the shear-wave velocity anomalies at the source locations. For this purpose, we use both the helium and lead isotopic compositions of OIBs. The helium isotopic compositions of OIBs are used to identify the source region hosting primitive $^4He/^3He$ material in the mantle, for example, whether the primitive helium isotopic composition of OIBs is restricted to the only seismically slow regions in the lowermost mantle. The lead isotopic composition is used to further test this hypothesis and evaluate the distribution of recycled materials in the lower mantle.

2. Materials and Methods

Section 2.1 describes the methods for new laboratory measurements of helium isotope ratios from OIB samples. Sections 2.2 describes the geodynamic models used to predict the plume source locations in the lower mantle. Section 2.3 describes the statistical methods employed to evaluate the relationships between helium and lead isotope ratios and deep mantle shear-wave velocity anomalies.

2.1. Helium Isotope Analyses

New helium isotopic compositions were determined for two samples from Marion Island and six samples from the Balleny Islands. These new analyses allow us to expand the global database of helium isotopes and, in the case of the Balleny Islands, evaluate the helium isotopic composition of regions of the mantle far removed from the LLSVPs. Approximately 0.109 to 1.077 g of olivine was picked for helium isotopic analyses following the methods of Parai et al. (2009). The olivine grains were loaded into a piston crusher and crushed under vacuum using a hydraulic ram to release magmatic gases trapped in fluid and melt inclusions. The total duration of each crushing step was less than 5 min. The evolved gases were purified by sequential exposure to hot and cold SAES getters, and noble gases (except for helium) were trapped on a cryogenic cold finger at 33 K. Helium was let into a Nu Noblesse noble gas mass spectrometer. Helium-4 was measured on a Faraday cup (15 s for nine cycles), and ^3He was measured using an ETP discrete dynode multiplier operating

Table 1
Helium Isotopic Composition for the Balleny Islands and Marion Island

Location	Sample name	Mass (g)	[^{4}He] (10^{-9} cm^3 STP/g)	^{4}He/^{3}He	±1σ
Marion Island	LC-128	0.433	15.78	93,300	1,700
Marion Island	LC-111	0.740	8.36	91,870	1,600
The Balleny Islands–Sturgis Island	B13722	1.077	4.70	125,600	4,600
The Balleny Islands–Sturgis Island	B13719	0.830	1.09	120,100	7,100
The Balleny Islands–Sabrina Island	B13715	0.532	20.34	105,800	2,000
The Balleny Islands–Sabrina Island	B13700	0.109	46.18	108,000	4,100
The Balleny Islands–Sabrina Island	B13710	0.464	10.81	113,000	4,300
The Balleny Islands–Young Island	YI-7	0.414	1.03	120,100	6,113

in pulse counting mode. The multiplier used for measuring ^{3}He is located on-axis and equipped with an energy filter to reduce scattered ions. Typical crusher blank values were ~1–2 × 10^{-11} cm^3 ^{4}He STP, or 0.1–1.0% of the typical measured signal. Helium isotopic ratios and concentrations were determined by normalizing to a standard that was prepared at Harvard (HH3; Gayer et al., 2008). The 2σ variability of standards with He concentrations similar to that of the samples was 0.7–12.0% for the ^{4}He/^{3}He ratio and ≤9.5% for ^{4}He abundance. The helium isotopic composition for samples from Marion Island and the Balleny Islands is reported in Table 1. Additional geochemical information about the samples can be found in le Roex et al. (2012) for Marion Island and Green (1992) and Lanyon et al. (1993) for the Balleny Islands. Supporting information Table S1 reports a global compilation of minimum ^{4}He/^{3}He ratio per ocean island or seamount track including our new data from both Marion and the Balleny Islands (see also supporting information).

2.2. Geodynamic Modeling of Plume Source Locations

Models for the evolution of plume conduit shapes were carried out in two steps. First, models of mantle flow were run backward in time, solving only the advection equation, assuming only depth-dependent viscosity, incompressible flow, and neglecting the influence of phase transitions. Second, forward-in-time models for the evolution of plume conduit shape were run following closely the methodology of Steinberger and O'Connell (1998) and Steinberger (2000). Below we provide a complete description of the methodology and identify where our methodology differs from what has been done previously.

Backwards-in-time mantle flow models were carried out using CitcomS 3.1.1 (Zhong et al., 2008, 2000) with a resolution of 65 × 65 × 65 elements on each of the 12 spherical caps. All models were calculated for a nominal value of the Rayleigh number of 2×10^7, defined in the CitcomS convention with Earth's radius as the characteristic length scale. We used a depth-dependent viscosity with simplified radial viscosity structures (Table 2 and Figure S1) defined by constant viscosities within the lithosphere (η_{lith}), upper mantle (η_{um}), lower mantle (η_{lm}), and lowermost mantle (η_{tbl}). The depth of the increase in viscosity between the upper mantle and lower mantle (LM/UM depth in Table 2) was varied between 660 and 1,000 km. The backward-in-time models were initialized at present day using a mantle tomography model, here either the V_S tomography model SEMUCB-WM1 (French & Romanowicz, 2015) in the series of models whose labels begin with model1 or the V_S tomography model S40RTS (Ritsema et al., 2011) in the models whose labels begin with model2. Shear-wave velocity anomalies were converted to density anomalies using a linear scaling factor $d\ln\rho/d\ln V_S = 0.2$, and then density anomalies were converted to temperature anomalies by assuming a constant linear coefficient of thermal expansion $\alpha = 3 \times 10^{-5}$ K^{-1}. We also performed a thermochemical calculation (model1-tc1) in which regions having shear velocity slower than −1.5% in the lowermost 200 km of the mantle were assigned zero buoyancy, implying a balance between thermal and compositional buoyancy. To run the models backward in time, the sign of the buoyancy was reversed such that seismically slow anomalies become positive density anomalies. Free-slip boundary conditions were imposed at the core mantle boundary, while time-dependent plate motions from the plate reconstruction of Seton et al. (2012) for the past 200 Myr were imposed at the surface.

The forward-in-time evolution of plume conduits was treated using a physically simplified model of plume conduit motion. Plume conduits were constructed as idealized “chains” of linear elements connected by

Table 2
Parameters for Plume Motion Models

Case	Tomography model	η_{lith}	η_{um}	η_{lm}	η_{tbl}	LM/UM depth (km)	τ_{adv} (myr)	V_{rise} (cm/year)
case1-0	SEMUCB-WM1[a]	1.00	0.01	1.00	0.1	1,000	45	2.2
case1-0	SEMUCB-WM1[a]	1.00	0.01	1.00	0.1	1,000	68	2.2
case1-0	SEMUCB-WM1[a]	1.00	0.01	1.00	0.1	1,000	75	2.2
case1-0	SEMUCB-WM1[a]	1.00	0.01	1.00	0.1	1,000	68	1.1
case1-0	SEMUCB-WM1[a]	1.00	0.01	1.00	0.1	1,000	68	4.4
case1-150x	SEMUCB-WM1[a]	1.00	0.00667	1.00	0.1	1,000	68	2.2
case1-50x	SEMUCB-WM1[a]	1.00	0.02	1.00	0.1	1,000	68	2.2
case1-660	SEMUCB-WM1[a]	1.00	0.01	1.00	0.1	660	68	2.2
case1-notbl	SEMUCB-WM1[a]	1.00	0.01	1.00	N/A (1.0)	1,000	68	2.2
case1-tc	SEMUCB-WM1[a]	1.00	0.01	1.00	0.1	1,000	68	2.2
case2-0	S40RTS[b]	1.00	0.01	1.00	0.1	1,000	45	2.2
case2-0	S40RTS[b]	1.00	0.01	1.00	0.1	1,000	68	2.2
case2-0	S40RTS[b]	1.00	0.01	1.00	0.1	1,000	75	2.2
case2-0	S40RTS[b]	1.00	0.01	1.00	0.1	1,000	68	1.1
case2-0	S40RTS[b]	1.00	0.01	1.00	0.1	1,000	68	4.4
case2-150x	S40RTS[b]	1.00	0.00667	1.00	0.1	1,000	68	2.2
case2-50x	S40RTS[b]	1.00	0.02	1.00	0.1	1,000	68	2.2
case2-660	S40RTS[b]	1.00	0.01	1.00	0.1	660	68	2.2
case2-notbl	S40RTS[b]	1.00	0.01	1.00	N/A (1.0)	1,000	68	2.2

Note. Viscosities (η) are nondimensional. Cases with a low-viscosity lowermost mantle ("tbl") have a viscosity reduction at 2,750-km depth. Thermochemical case ("tc") has removed all buoyancy from regions with dVs less than −1.5% in the lowermost mantle, reflecting a balance between thermal and compositional buoyancy in the large low shear-wave velocity provinces. LM = lower mantle; UM = upper mantle; N/A = not applicable.
[a]French and Romanowicz (2015). [b]Ritsema et al. (2011).

vertices. These elements can be advected laterally by mantle flow, and they rise radially due to a combination of mantle flow and an excess buoyant rise velocity that is inversely proportional to the local mantle viscosity. A large population of candidate plume conduits were initially introduced into the models, with base locations on a regular (degree-by-degree) grid. At each time step, each plume conduit element moved with a velocity

$$\underline{v}_p = \underline{v} + v_{rise}\hat{\underline{e}}_r,$$

where $\underline{v}_p$ is the (vector) plume conduit velocity, $\underline{v}$ is the local mantle flow velocity (which varies in space and time), and v_{rise} is an excess vertical rise speed, given by $v_{rise} = v_0 \frac{\eta_0}{\eta}$, and $\hat{\underline{e}}_r$ is a unit vector in the radial direction. The excess vertical rise speed (v_{rise}) is an expected physical behavior because plume conduits are hotter than and therefore more positively buoyant with respect to the ambient mantle. In the expression for v_{rise}, v_0 is the rising speed of the plume conduit element through ambient mantle with viscosity η_0. Unless stated otherwise (e.g., Table 2), the reference rise velocity (this is the value of v_{rise} when the background mantle viscosity is 10^{21} Pa·s) is chosen as 2.2 cm/year, for consistency with Steinberger and O'Connell (1998). The local mantle flow velocity ($\underline{v}$) was evaluated from the output of the backward-in-time mantle circulation model, and plume conduits were allowed to evolve in the time-varying velocity field. When plume conduits became tilted more than 60° relative to vertical, they were beheaded. This was accomplished by splitting the plume conduit "chain" into two separate plume conduits. The lower portion of a beheaded plume was allowed to persist and continue to evolve since it was still connected to the lower thermal boundary layer, but the upper portion of a beheaded plume becomes extinct. When plume conduits rose to a depth of less than 150 km (the base of the lithosphere), they were truncated. In order to maintain adequate numerical resolution of plume conduits, additional elements were added by bifurcation whenever the vertical extent of a plume conduit element exceeds 55.5 km (Steinberger & O'Connell, 1998).

The goal of exploring plume models based on these different model parameterization choices was to identify the range of possible outcomes, given significant uncertainties in present-day mantle structure and rheology. Our backward-in-time models differ from those of Steinberger and O'Connell (1998) and Steinberger (2000) in that these new mantle flow models were carried out using the finite element code CitcomS instead of using a propagator matrix method. Our backward-in-time models also employed

different mantle tomography models to form the initial condition and used the plate reconstruction of Seton et al. (2012) instead of the reconstruction by Lithgow-Bertelloni and Richards (1998). These new models also allow us to explore the relationship of geochemistry to the deep mantle for hotspots that were not previously modeled (e.g., Marion and the Balleny Islands). The model setup parameters are given in Table 2, and the predicted source location (latitude and longitude at a depth of 2,850 km) for each plume is reported in Table S1.

2.3. Determining the Relationship Between Isotope Ratios and Shear-Wave Velocities

To evaluate potential links between isotope ratios ($^4He/^3He$ and $^{208}Pb^*/^{206}Pb^*$) and seismically observed deep mantle structures, we first characterized the magnitude and sign of shear-wave velocity anomalies at the predicted base location of each plume conduit. The radii of plume conduits are characterized by some finite width, and therefore, plumes sample their source regions over an area that may be characterized by a distribution of shear-wave velocity anomalies. To test the sensitivity of our results to these potential variations, we determined the magnitude and sign of shear-wave velocity anomalies using both the mean and minimum values of shear-wave velocity anomalies that are within 2° and 5° of the base of each plume.

Many OIBs such as Iceland, Hawaii, Galápagos, and Samoa display a wide range of geochemical compositions (e.g., $^4He/^3He$ and $^{208}Pb^*/^{206}Pb^*$ ratios) both spatially and temporally. The geochemical variability observed within individual ocean island tracks present time-dependent admixtures of various mantle components with the most extreme values providing the closest match to "true" end-member compositions. For example, the lowest $^4He/^3He$ ratios in individual hotspots reflect the closest analog of the most primitive material in the plume source, while the highest $^{208}Pb^*/^{206}Pb^*$ ratios are the closes analog of the composition of the enriched materials such as oceanic crust that are recycled back into the Earth's mantle. Because the purpose of the present work is to understand whether the primitive materials are restricted to specific regions in the lower mantle (e.g., low shear-wave velocity regions) or more broadly distributed in the lower mantle, we use minimum $^4He/^3He$ and maximum $^{208}Pb^*/^{206}Pb^*$ ratios to characterize the relationship between seismic velocities and helium and lead isotopic compositions from each ocean island or seamount track.

The relationship between the shear-wave velocity anomalies at the base of the plume conduits and surface geochemistry was then evaluated using two different approaches:

1. In the first approach, we explored whether plumes with specific geochemistries (e.g., primitive low $^4He/^3He$ ratios) are sourced from the seismically slow ($dVs < 0$) or fast ($dVs > 0$) regions of the lowermost mantle. To do this, plume conduits that are rooted in seismically slow regions were grouped together, while plume conduits that are rooted in seismically fast regions were assigned to a second group. We then compared the distributions of plume geochemistry (minimum $^4He/^3He$ and maximum $^{208}Pb^*/^{206}Pb^*$ ratios) for those two groups to determine whether plumes with, for example, primitive low $^4He/^3He$ ratios are sourced from the seismically slow ($dVs < 0$) or fast ($dVs > 0$) regions of the lowermost mantle. The distributions of plume geochemistry were evaluated using kernel density functions assuming a bandwidth of 8,000 and 0.05 for minimum $^4He/^3He$ and maximum $^{208}Pb^*/^{206}Pb^*$ ratios, respectively. Each curve represents a single model result from Table 2, which results in 10 red and blue curves in Figure 1 and nine red and blue curves in Figure 2 (there are only nine in Figure 2 because a thermochemical simulation was not run using the S40RTS models).
2. In the second approach, we explored whether the geochemical variability observed in OIBs reflects linear mixing of chemically distinct materials from seismically distinct mantle reservoirs. Our rationale for exploring a linear relationship is the (simplified) expectation that shear-wave velocities relate to temperatures and the buoyancy of mantle materials; for example, slower shear-wave velocity anomalies may be related to higher temperatures and, therefore, higher buoyancies. In this case, plumes would be composed of a higher proportion of primitive material if low $^4He/^3He$ ratios were derived from the seismically slowest regions of the lower mantle. We examined the significance of potential linear relationships by calculating the Pearson correlation coefficient between isotope ratios (either minimum $^4He/^3He$ or maximum $^{208}Pb^*/^{206}Pb^*$ ratios) and shear-wave velocity anomalies at the source of each plume conduit. The results are displayed as white circlesin Figures 1–2 that represent the Pearson correlation coefficient calculated from the results of each flow model from Table 2.

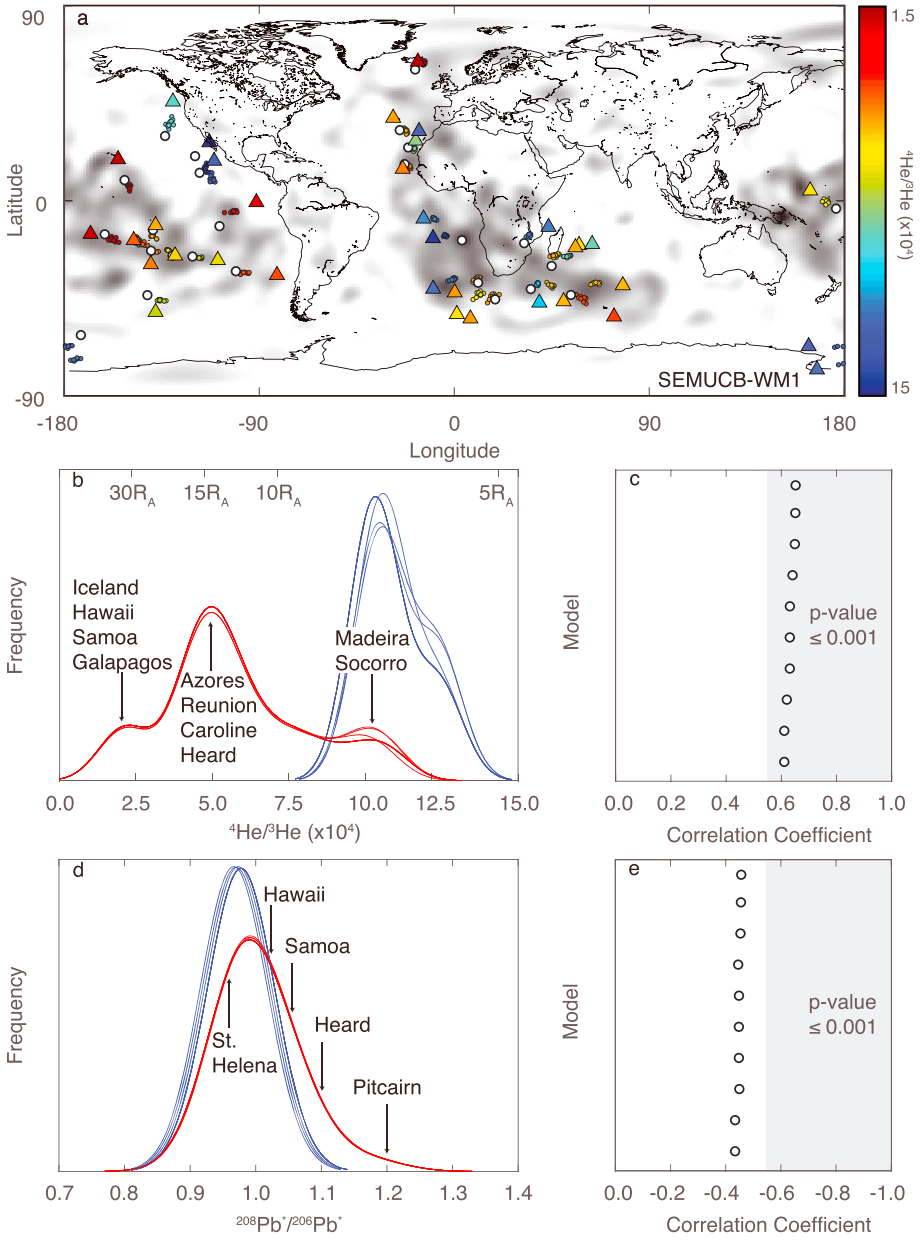

Figure 1. Relationship between surface geochemistry and shear-wave velocity anomalies in the lowermost mantle using the tomography model SEMUCB-WM1 (French & Romanowicz, 2015). (a) The predicted lateral offset of plume source locations from their surface expressions when large-scale mantle flow is taken into account. Gray regions depict slower than average shear-wave velocity of the lowermost mantle (at 2,850-km depth), highlighting the geographic extent of the two LLSVPs for the tomography model SEMUCB-WM1 (French & Romanowicz, 2015). Triangles represent the current-day surface location of hotspots, whereas circles represent the base location of the plume conduits predicted by back-advection calculations as described in section 2.2. The fill color of the triangle and circles denote the lowest $^{4}He/^{3}He$ ratio measured at a single hotspot or within a single hotspot track. Warmer colors indicate lower $^{4}He/^{3}He$ ratios, while cooler colors are characteristic of relatively high $^{4}He/^{3}He$ ratios. Color bar is on a linear scale. Plume conduit base locations predicted by Steinberger and Antretter (2006) and Boschi et al. (2007) are shown here as large white circles. Note the similarity in lateral offset between plume base locations and their surface expressions predicted here in our study and those predicted by Steinberger and Antretter (2006) and Boschi et al. (2007). Display frequency diagrams showing the distribution of (b) $^{4}He/^{3}He$ (excluding Tristan-Gough, St. Helena) and (d) $^{208}Pb^{*}/^{206}Pb^{*}$ ratios for plume conduits that are sourced from seismically fast regions (blue curves) and seismically slow (red curves) regions of the lowermost mantle. Each curve represents a single model result from Table 2. Given this, there are 10 red curves and 10 blue curves in Figure 1. The white circles represent the distribution of correlation coefficients between (c) $^{4}He/^{3}He$ and (e) $^{208}Pb^{*}/^{206}Pb^{*}$ ratios of plumes and shear-wave velocities at 2,850 km. The gray shaded region denotes correlation coefficients that are considered significant at a p value of 0.001. Note the strong relationship between $^{4}He/^{3}He$ ratios and shear-wave velocities in the lowermost mantle. Conversely, maximum $^{208}Pb^{*}/^{206}Pb^{*}$ ratios display no significant relationship with shear-wave velocities in the lowermost mantle at a p value of 0.001.

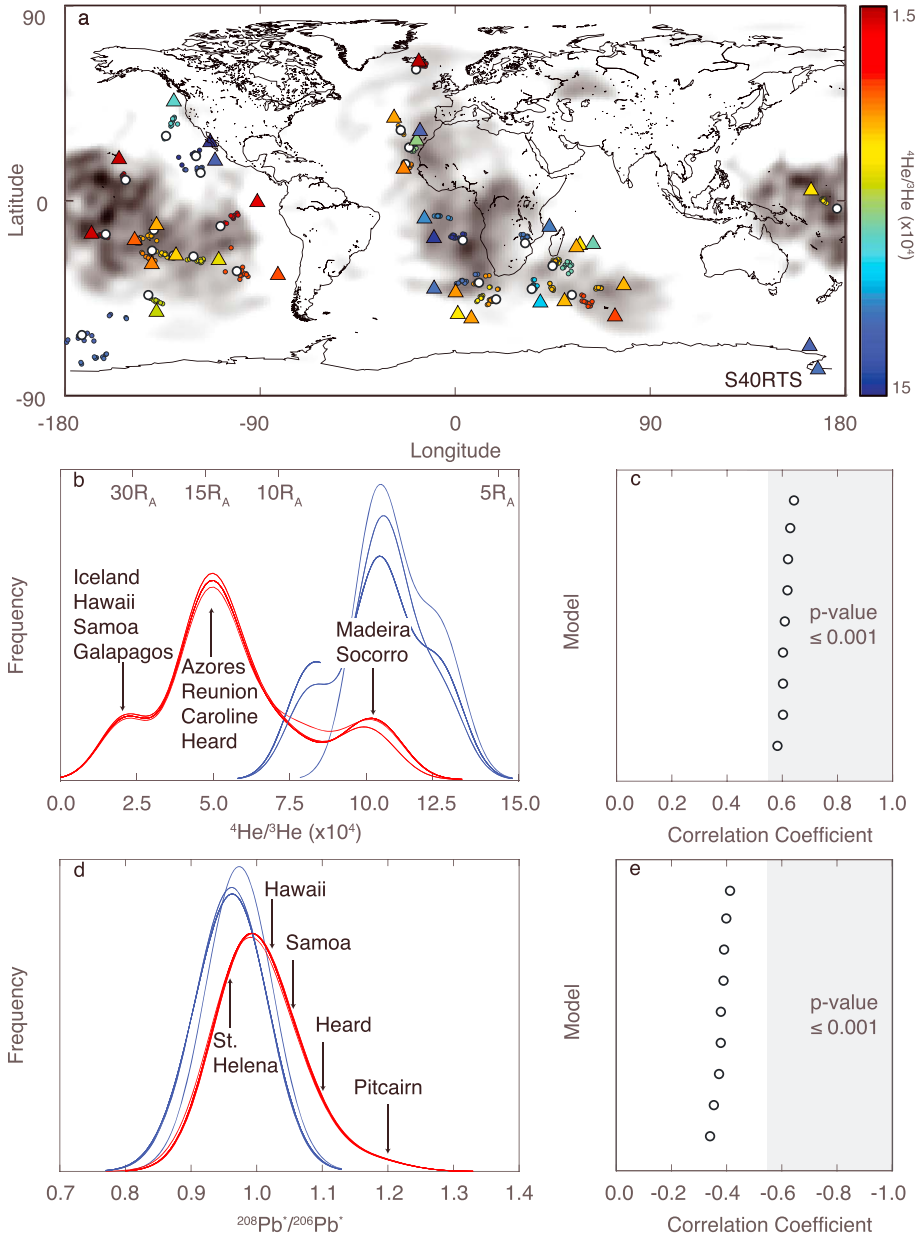

Figure 2. Relationship between surface geochemistry and shear-wave velocity anomalies in the lowermost mantle using the tomography model S40RTS (Ritsema et al., 2011). (a–e) Same as in Figure 1. Note a significant correlation is observed between minimum $^{4}He/^{3}He$ ratios (but not maximum $^{208}Pb^{*}/^{206}Pb^{*}$ ratios) and shear-wave velocity anomalies when lateral is taken into account.

3. Results

The relationship between the surface geochemistry of oceanic basalts and mantle shear-wave velocity anomalies (based on both kernel density estimates and Pearson correlation coefficients) are presented below. Section 3.1 describes the predicted plume source locations based on our geodynamic models. Sections 3.2 describes the relationship between minimum $^{4}He/^{3}He$ ratios and shear-wave velocities. Section 3.3 describes the relationship between maximum $^{208}Pb^{*}/^{206}Pb^{*}$ ratios and shear-wave velocities.

3.1. Predicted Plume Source Locations

Figures 1a and 2a show the predicted lateral offset of plume source locations in the lower mantle from their surface expressions when large-scale mantle flow is taken into account using the SEMUCB-WM1 (Figure 1)

and S40RTS (Figure 2) tomographic models. All of the mantle flow models predict large-scale convergence of flow in the lower mantle toward the central Pacific and Africa (the locations of the LLSVPs) due to subduction of circum-Pacific slabs. In all models, the strongest lateral deflection occurs in the upper mantle where plume conduits are influenced by plate motions. This lateral deflection of plumes results in surface expressions that no longer overlie the lower mantle source location initially sampled by these plumes. The mantle flow models also predict that the source regions for the Balleny Islands Mount Erebus, Guadalupe Island, and the Cobb hotspot track are located in seismically faster regions of the lowermost mantle, that is, outside of the LLSVPs. These results are only weakly sensitive to different model parameterizations (Table 2) including tomography model, radial viscosity structure, advection timescale, and transport properties. The predicted lateral offset of plume source locations in the lower mantle from their surface expressions predicted here are consistent with results from previous models of plume dynamics (Boschi et al., 2007, 2008; Steinberger, 2000; Steinberger & Antretter, 2006; Steinberger & O'Connell, 1998; Steinberger et al., 2004).

3.2. Relationship Between Minimum $^4He/^3He$ Ratios and Shear-Wave Velocities

Figures 1b, 1c, 2b, and 2c demonstrate that the distribution of minimum $^4He/^3He$ ratios in the deep mantle is not random. Figures 1b and 2b show that basalts derived from anomalously slow seismic regions in the lowermost mantle are associated with the most primitive helium isotopic signatures. The first group shown in red contains plume conduits that are sourced from slower than average shear-wave velocities ($dVs < 0$) located within the two LLSVPs and their erupted products are characterized by relatively low (primitive) $^4He/^3He$ ratios (e.g., Iceland $^4He/^3He_{max} = 19{,}060$; Hawaii $^4He/^3He_{max} = 20{,}360$; Samoa $^4He/^3He_{max} = 20{,}950$; Galápagos $^4He/^3He_{max} = 23{,}720$). These observations indicate that primitive (low) $^4He/^3He$ ratios are associated with slow shear-wave velocities and never associated with fast shear-wave velocities. In general, most plume conduits rooted in seismically slow regions lie within the lateral extent of the LLSVPs (e.g., Burke et al., 2008); thus, primitive (low) $^4He/^3He$ ratios appear to be confined to the LLSVPs. However, it should be noted that recent tomographic images indicate that the LLSVPs may not be contiguous features but may be composed of multiple subdomains (French & Romanowicz, 2015). Therefore, the extent of the LLSVPs may be a bit uncertain, but the long-wavelength structure shows fairly good agreement between all models (Cottaar & Lekic, 2016).

The second group of plume conduits depicted by blue curves are sourced from faster than average shear-wave velocities in the lowermost mantle and are characterized by relatively high (radiogenic) $^4He/^3He$ ratios. For example, the $^4He/^3He$ ratios in the Balleny Islands range from 105,800 to 125,600 and are predicted here to be sourced from seismically fast regions in the lower mantle. Intraplate volcanism represented by Mount Erebus, Guadalupe Island, and (in some mantle flow simulations) the Cobb hotspot track are also located outside regions bounded by the LLSVPs and are characterized by $^4He/^3He$ ratios greater than ~81,940 (approximately $^3He/^4He = 8.8\ R_A$; Eiler et al., 1997; Lupton et al., 1993; Parmelee et al., 2015). Figures 1c and 2c show that the minimum $^4He/^3He$ ratios of plumes display a significant positive relationship (given $p \leq 0.001$) with shear-wave velocities at 2,850 km such that primitive $^4He/^3He$ ratios are associated with relatively slow shear-wave velocities, while radiogenic $^4He/^3He$ ratios are associated with relatively fast shear-wave velocities.

Figures 1, 2 exclude two hotspot locations (Tristan-Gough, St. Helena) where basalts with the most primitive $^4He/^3He$ ratios still contain significant amounts of recycled materials (Class & le Roex, 2008; Kawabata et al., 2011; Willbold & Stracke, 2006, 2010). It has been shown that HIMU-type basalts, which have relatively radiogenic helium isotopic compositions, also have less nucleogenic neon (Hilton et al., 2000; Parai et al., 2009), requiring the presence of primitive material in their source region (Day & Hilton, 2011; Hilton et al., 2000; Parai et al., 2009). Given this, the helium isotopic composition of these basalts may not accurately reflect the primitive nature of their source regions. However, the overall results do not significantly change if these basalts are included (see Figure S1). Figure S1 also shows the results are insensitive to the sampling strategy used to determine the sign and magnitude of the shear-wave velocity anomaly at the base of each plume conduit.

Figure S3 shows the relationship between minimum $^4He/^3He$ ratios of plumes and shear-wave velocities for intraplate volcanism most closely associated with the African LLSVP and the Pacific LLSVP. While the Pacific LLSVP appears to show a stronger overall correlation, the relationship between minimum $^4He/$

^{3}He ratios of plumes and shear-wave velocities for plumes associated with the African LLSVPs completely overlap, that is, display a similar range and relationship when minimum ^{4}He/^{3}He ratios is plotted against shear-wave velocities. Therefore, it may be a bit premature to conclude that this is reflective of similarities or differences between the two LLSVPs. Furthermore, if these two regions of the mantle turn out to be statistically distinct, it could also reflect differences in entrainment processes or the history of subduction into the different ocean basins. Future work is required to investigate whether these preliminary observations are robust.

3.3. Relationship Between Maximum $^{208}Pb^{*}/^{206}Pb^{*}$ Ratios and Shear-Wave Velocities

Contrary to the predicted relationship between minimum ^{4}He/^{3}He ratios and shear-wave velocities, Figures 1d, 1e, 2d, and 2e demonstrate that there is no significant relationship between the distribution of maximum $^{208}Pb^{*}/^{206}Pb^{*}$ ratios and shear-wave velocities in the deep mantle. For example, Figures 1d and 2d show that lower mantle materials do not separate into two distinct groups based on the relationship between shear-wave velocities and maximum $^{208}Pb^{*}/^{206}Pb^{*}$ ratios. Both red and blue curves display similar median values and variances, indicating that end-member $^{208}Pb^{*}/^{206}Pb^{*}$ ratios are just as likely to be found in relatively fast and slow shear-wave velocities of the lowermost mantle. Figures 1e and 2e demonstrate there is no significant linear relationship between maximum $^{208}Pb^{*}/^{206}Pb^{*}$ ratios of plumes and shear-wave velocities at 2,850 km as all of the simulations result in correlation coefficients that are not significant at a p value of 0.001.

4. Discussion

The low ^{4}He/^{3}He ratios in many OIBs provide evidence for the preservation of primitive material in the Earth's mantle; however, the geographical location of the primitive deep mantle reservoir(s) remains unknown. The simulations of mantle flow used to trace the geochemistry of individual ocean islands to their source location in the lower mantle suggests that primordial helium is spatially restricted to the LLSVPs, while radiogenic lead is distributed more broadly throughout the mantle. These results build on the prediction of plume deflection using backward-in-time models of large-scale mantle flow and forward models of the interaction of small-scale plumes with the large-scale flow. These results depend on the inferred buoyancy structure, viscosity structure, and kinematic boundary conditions. Our models span a range of plausible mantle viscosities, plume buoyancies, and mantle buoyancy structures, all of which affect the predicted plume shapes. Thus, the details of the predicted plume shapes remain somewhat uncertain, though the overall direction and amount of deflection are in good agreement among all of our models. A confirmation of plume shapes from improved mantle tomography models would reinforce our conclusions, as would more detailed comparisons between the plume shapes predicted using the backward- and forward-in-time models for plume dynamics employed here and the plume morphology in fully dynamical simulations of mantle convection.

4.1. The Mantle Source Region of Primitive (Low ^{4}He/^{3}He) Materials

The lower ^{4}He/^{3}He ratios associated with ocean islands reflect low time-integrated (U + Th)/^{3}He ratios associated with less processed, more primitive mantle reservoirs. Figures 1 and 2 demonstrate that the distribution of minimum ^{4}He/^{3}He ratios in the deep mantle is not random because primitive ^{4}He/^{3}He ratios in the deep mantle are geographically restricted to only the seismically slow regions above the core-mantle boundary (e.g., LLSVPs). In contrast, reconstructed plume source locations that lie within these seismically fast regions display a peak in ^{4}He/^{3}He ratio of ~100,000, which is on the upper end of the typical MORB range of ~80,000–103,000 (e.g., Graham, 2002; Moreira, 2013). Thus, regions in the lowermost mantle that lie outside of the LLSVPs likely share a geochemical evolution similar to that of the typical MORB source, at least in its helium isotopic composition. Since the observed peak of ~100,000 is slightly more radiogenic than the average MORB (^{4}He/^{3}He ~88,000), it is likely that there is a higher proportion of recycled material in the ambient deep mantle compared to the shallow upper mantle sampled beneath mid-ocean ridges. Conversely, the lack of any correlation between maximum $^{208}Pb^{*}/^{206}Pb^{*}$ ratios and shear-wave velocity anomalies in the lower mantle (see Figures 1d, 1e, 2d, and 2e) demonstrates that recycled materials are not geographically restricted to only regions defined by the LLSVPs but are distributed more broadly across the lowermost mantle.

While we have assumed that plumes predicted to be rooted in seismically fast regions are derived from the lower mantle, such plumes may not be rooted at the core-mantle boundary. Future high-resolution seismic imaging of these regions is needed to discern whether these materials are indeed sourced from the lower mantle. However, it should be noted that primitive helium is only associated with seismically slow regions in the lower mantle; whether plumes predicted to be rooted in seismically fast regions actually have a deep mantle origin or not does not change this conclusion. Furthermore, if the seismically fast regions of the lower mantle are not sampled by plumes, then these seismically fast regions represent a geochemically hidden reservoir.

The geographical restriction of primitive $^4He/^3He$ ratios to seismically slow regions at the bottom of the mantle allows us to evaluate additional hypotheses regarding the distribution and origin of primitive (low $^4He/^3He$) reservoirs within the Earth. For example, it has been suggested that primitive helium could be distributed as isolated blobs of material throughout the mantle (Becker et al., 1999). This proposal was motivated by calculations that showed high-viscosity blobs could persist for long periods of Earth's history without becoming mixed into the ambient mantle (Manga, 1996). However, such a scenario would not lead to strong correlations between minimum $^4He/^3He$ ratios and seismically slow shear-wave velocities in the lowermost mantle. Alternatively, bridgmanite-enriched regions of the mantle (BEAMS) have also been proposed to host primitive, low $^4He/^3He$ materials (Ballmer et al., 2017). In this scenario, upwelling (i.e., plumes) occurs between the slowly rotating BEAMS, so one would not expect a correlation between BEAMS and the location of plume roots or conduits. Plumes could conceivably entrain primitive BEAMS material on their way up through the lower mantle; however, it is unlikely that this process would be significant, given the high viscosity contrast between BEAMS and plumes (Manga, 1996).

The core has also been considered as a possible source of helium with low $^4He/^3He$ ratios (Bouhifd et al., 2013; Jephcoat, 1998; Porcelli & Halliday, 2001) where diffusion of helium from the outer core into the thermal boundary layer at the base of the mantle supplies the primitive helium sampled by plumes. While recent experimental results display the capacity for dissolving sufficient helium into iron metal (e.g., Bouhifd et al., 2013; Jephcoat, 1998), these experiments do not directly inform us that sufficient helium was in fact sequestered in the core or that helium is actually diffusing from the core into the thermal boundary layer. Primitive helium diffusing out of the core would be expected to produce low $^4He/^3He$ ratios in the lower thermal boundary layer, but there is no a priori expectation for helium diffusion out of the core to be localized in LLSVPs. Helium diffusion from the core would also be expected to produce low $^4He/^3He$ ratios in hotspots derived from parts of the thermal boundary layer outside the region defined by the LLSVPs. This is not observed, though more comprehensive sampling of these hotspots and their tracks is warranted.

The results presented here do not rule out the possibility of ultralow velocity zones (ULVZs) as the source of primitive materials characterized by low $^4He/^3He$ ratios and other isotopic anomalies (Mundl et al., 2017; Yuan & Romanowicz, 2017). For example, low $^4He/^3He$ materials may be sourced from a thin, partially molten layer at the base of the mantle. This layer may be dynamically focused into small hills that are subsequently entrained into plumes (Yuan & Romanowicz, 2017). However, the limited height and/or lateral extent of all but the largest of these structures (the mega-ULVZs; Cottaar & Romanowicz, 2012; Thorne et al., 2013; Yuan & Romanowicz, 2017) may prevent them from currently being imaged seismically. Alternatively, ULVZ material may be viscously mixed into the LLSVPs (Li et al., 2017), which could also account for the strong correlation between minimum $^4He/^3He$ ratios and seismically slow shear-wave velocities in the lowermost mantle. Testing of these scenarios requires, for example, further characterization of the lowermost mantle's small-scale structure with particular emphasis on whether ULVZs are present at the base of other mantle plume conduits (Yuan & Romanowicz, 2017).

4.2. Formation and Evolution of the LLSVPs

The primitive (low $^4He/^3He$) nature of seismically slow shear-wave velocity structures in the lowermost mantle indicates that the LLSVPs cannot be composed entirely of recycled slabs (Castillo, 1988; Farnetani et al., 2012; Harpp et al., 2014; Harrison et al., 2017; Hoernle et al., 2015; Huang et al., 2011; Payne et al., 2013; Tackley, 2011; Tan & Gurnis, 2005; Weis et al., 2011), as recycled slabs have radiogenic (high $^4He/^3He$) signatures and would not produce materials with low $^4He/^3He$ ratios. It is possible that the LLSVPs represent a single geochemical component with a uniformly low $^4He/^3He$ ratio and the correlations

observed in this study represents two-component mixing between this primitive material that is geographically restricted to the LLSVPs and a more radiogenic component of the ambient mantle during plume entrainment. However, the primitive (low $^{4}He/^{3}He$) signature of the LLSVPs does not preclude some amount of recycled materials from being incorporated into this reservoir through geologic time, but this recycled component may represent only a minor fraction of the LLSVPs. This is consistent with Li et al. (2014) who use numerical simulations of mantle convection to investigate interactions between a primitive (and intrinsically more dense) lower mantle reservoir with deeply subducted materials. These simulations show that a small fraction of the total recycled material in the mantle can be convectively stirred into a more dense primitive reservoir, while the balance of recycled material remains within the ambient (lower) mantle (Li et al., 2014). Therefore, the LLSVPs may be a multicomponent mixture of materials of different origins that are characterized by distinct geochemistries.

Extinct radionuclide systems, such as the ^{129}I-^{129}Xe and ^{182}Hf-^{182}W isotope systems, provide important chronologic constraints on the formation of the LLSVPs. Short-lived ^{129}I (half-life of 15.7 million years) and ^{182}Hf (half-life of 8.9 million years) decay to ^{129}Xe and ^{182}Hf with the two radionuclides becoming extinct 100 and 60 million years after the start of the solar system, respectively. Consequently, ^{129}Xe or ^{182}W isotopic anomalies in mantle reservoirs can only be generated during the first 100 and 60 million years after the start of the solar system. Isotopic anomalies in ^{129}Xe have been observed in low $^{4}He/^{3}He$ materials at Iceland and in the Rochambeau Bank where the Samoan plume is sampled (Mukhopadhyay, 2012; Pető et al., 2013). Since these plumes are rooted in the LLSVPs, the presence of the ^{129}Xe anomalies require the LLSVPs to have formed prior to ^{129}I becoming extinct, that is, no later than 100 million years after the start of the solar system. Furthermore, because $^{129}Xe/^{130}Xe$ ratios in the plume and MORB sources are distinct in the modern-day mantle, the two sources must have remained separated for at least the past 4.45 billion years (Mukhopadhyay, 2012; Pető et al., 2013). Similarly, isotopic anomalies in ^{182}W (due to the decay of ^{182}Hf) have also been observed in low $^{4}He/^{3}He$ materials (Mundl et al., 2017; Rizo et al., 2019). Given its even shorter half-life, ^{182}W anomalies in low $^{4}He/^{3}He$ materials (Mundl et al., 2017; Rizo et al., 2019) require that the low $^{4}He/^{3}He$ reservoir was generated no later than 60 million years after solar system formation (though we do note that the validity of some tungsten isotope data in low $^{4}He/^{3}He$ materials is still debated; Kruijer & Kleine, 2018; Rizo et al., 2016). The timing of the Moon-forming giant impact is still debated, although recent isotopic studies (Barboni et al., 2017) constrain Moon formation to between 50 and 60 million years after the start of the solar system (Barboni et al., 2017; Touboul et al., 2007). Given these chronologic constraints, the formation of LLSVPs likely predates the Moon-forming giant impact. If so, LLSVPs are not the product of a magma ocean generated by the Moon-forming giant impact. The formation of the LLSVPs is more likely associated with the creation of a primitive reservoir during previous episodes of magma ocean crystallization, which formed ancient reservoirs that subsequently survived the Moon-forming giant impact. This is consistent with the interpretations of Tucker and Mukhopadhyay (2014) based on the range of $^{3}He/^{22}He$ ratios observed in oceanic basalts.

The early formation and subsequent preservation of the LLSVPs indicates this primitive reservoir has also survived 4.5 billion years of mantle convection. This requires the LLSVPs to have limited interactions with the MORB source and with recycled material returned to the mantle via subduction. However, because the LLSVPs are being entrained by plumes, these reservoirs are being eroded as a function of time. Consequently, the reservoir must have comprised more than 1.6–9.4% of the Earth's total mantle by mass (estimates of the present-day LLSVP mass; Burke et al., 2008; Cottaar & Lekic, 2016) back in time. Assuming a constant plume buoyancy flux derived by King and Adam (2014) and that LLSVP material comprises 10% of that flux (e.g., Deschamps et al., 2011), we estimate that roughly 3–30% of the present-day LLSVP volume has been lost through entrainment processes over Earth's history, though plume fluxes were most likely higher in the past. The loss of LLSVP material due to entrainment may, however, be offset by the addition of recycled material throughout Earth's history.

5. Conclusions

We demonstrate that basalts with the most primitive helium isotopic signatures derive from the two continent-sized large low shear-wave velocity provinces (LLSVPs) by combining tomographic models, dynamic simulations of mantle flow, and a comprehensive helium isotopic data set of oceanic basalts. The

primitive (low $^4He/^3He$) signature of the LLSVPs indicates these regions are not composed entirely of recycled slabs. Furthermore, no significant relationship is observed between maximum $^{208}Pb^*/^{206}Pb^*$ ratios and seismically slow regions in the lowermost mantle, indicating recycled materials are more broadly distributed across the mantle. Xenon and tungsten isotopic anomalies associated with the primitive (low $^4He/^3He$) signature of the LLSVPs imply that these seismically slow regions must have formed during Earth's accretion and survived the Moon-forming giant impact along with nearly 4.5 billion years of mantle convection.

Acknowledgments
Thoughtful comments from Rhodri Davis and two anonymous reviewers are gratefully acknowledged, as is the editorial assistance of Thorsten Becker. This work is supported by the NSF Postdoctoral Fellowship (NSF EAR-PF-1349811 to C. D. Williams), NSF Petrology and Geochemistry program (NSF EAR-1450659 to S. Mukhopadhyay), NSF Marine Geology and Geophysics program (NSF OCE-1464484 to S. Mukhopadhyay), NSF Geophysics program (NSF EAR-1622464 and NSF EAR-1825104 to M. Rudolph), and NSF Geophysics program (NSF EAR-1345103 to B. Romanowicz), and computing resources were supported through NSF DMS-1624776 (to M. Rudolph) and Portland State University. Balleny samples were provided by Drs. Trevor H. Green and Jonathan H. Berg. Special thanks to Dr. P. Arriens who collected samples from Sturgis and Sabrina Islands on the Lewis Expedition to the Balleny Islands in 1978 and the crew of the U.S. Coast Guard Icebreaker "Polar Sea" and the Division of Polar Programs (NSF) for their support of J. H. Berg. The main data supporting the findings of this study are available within the article and its supporting information tables. This collaborative effort formed as a result of the 2014 and 2016 CIDER summer program, funded by the FESD NSF grant EAR-1135452.

References

Allègre, C.-J., Staudacher, T., Sarda, P., & Kurz, M. D. (1983). Constraints on evolution of Earth's mantle from rare gas systematics. *Nature*, *303*(5920), 762–766. https://doi.org/10.1038/303762a0

Ballmer, M. D., Houser, C., Hernlund, J. W., Wentzcovitch, R. M., & Hirose, K. (2017). Persistence of strong silica-enriched domains in the Earth's lower mantle. *Nature Geoscience*, *10*, 236–240. https://doi.org/10.1038/ngeo2898

Barboni, M., Boehnke, P., Keller, B., Kohl, I. E., Schoene, B., Young, E. D., & McKeegan, K. D. (2017). Early formation of the Moon 4.51 billion years ago. *Science Advances*, *3*, e1602365. https://doi.org/10.1126/sciadv.1602365

Becker, T. W., Kellogg, J. B., & O'Connell, R. J. (1999). Thermal constraints on the survival of primative blobs in th elower mantle. *Earth and Planetary Science Letters*, *171*(3), 351–365. https://doi.org/10.1016/S0012-821X(99)00160-0

Boschi, L., Becker, T. W., & Steinberger, B. (2007). Mantle plumes: Dynamic models and seismic images. *Geochemistry, Geophysics, Geosystems*, *8*, Q10006. https://doi.org/10.1029/2007GC001733

Boschi, L., Becker, T. W., & Steinberger, B. (2008). On the statistical significance of correlations between synthetic mantle plumes and tomographic models. *Physics of the Earth and Planetary Interiors*, *167*, 230–238. https://doi.org/10.1016/J.PEPI.2008.03.009

Bouhifd, M. A., Jephcoat, A. P., Heber, V. S., & Kelley, S. P. (2013). Helium in Earth's early core. *Nature Geoscience*, *6*(11), 982–986. https://doi.org/10.1038/ngeo1959

Bozdağ, E., Peter, D., Lefebvre, M., Komatitsch, D., Tromp, J., Hill, J., et al. (2016). Global adjoint tomography: First-generation model. *Geophysical Journal International*, *207*(3), 1739–1766. https://doi.org/10.1093/gji/ggw356

Burke, K., Steinberger, B., Torsvik, T. H., & Smethurst, M. A. (2008). Plume Generation Zones at the margins of large low shear velocity provinces on the core-mantle boundary. *Earth and Planetary Science Letters*, *265*(1-2), 49–60. https://doi.org/10.1016/j.epsl.2007.09.042

Castillo, P. (1988). The Dupal anomaly as a trace of the upwelling lower mantle. *Nature*, *336*(6200), 667–670. https://doi.org/10.1038/336667a0

Class, C., & le Roex, A. P. (2008). Ce anomalies in Gough Island lavas—Trace element characteristics of a recycled sediment component. *Earth and Planetary Science Letters*, *265*(3-4), 475–486. https://doi.org/10.1016/j.epsl.2007.10.030

Cottaar, S., & Lekic, V. (2016). Morphology of seismically slow lower-mantle structures. *Geophysical Journal International*, *207*(2), 1122–1136. https://doi.org/10.1093/gji/ggw324

Cottaar, S., & Romanowicz, B. (2012). An unsually large ULVZ at the base of the mantle near Hawaii. *Earth and Planetary Science Letters*, *355-356*, 213–222. https://doi.org/10.1016/j.epsl.2012.09.005

Day, J. M. D., & Hilton, D. R. (2011). Origin of $^3He/^4He$ ratios in HIMU-type basalts constrained from Canary Island lavas. *Earth and Planetary Science Letters*, *305*(1-2), 226–234. https://doi.org/10.1016/j.epsl.2011.03.006

Deschamps, F., Kaminski, E., & Tackley, P. J. (2011). A deep mantle origin for the primitive signature of ocean island basalt. *Nature Geoscience*, *4*(12), 879–882. https://doi.org/10.1038/ngeo1295

Eiler, J. M., Farley, K. A., Valley, J. W., Hauri, E. H., Craig, H., Hart, S. R., & Stolper, E. M. (1997). Oxygen isotope variations in ocean island basalt phenocrysts. *Geochimica et Cosmochimica Acta*, *61*(11), 2281–2293. https://doi.org/10.1016/S0016-7037(97)00075-6

Farley, K. A., Natland, J. H., & Craig, H. (1992). Binary mixing of enriched and undegassed (primitive?) mantle components (He, Sr, Nd, Pb) in Samoan lavas. *Earth and Planetary Science Letters*, *111*(1), 183–199. https://doi.org/10.1016/0012-821X(92)90178-X

Farnetani, C. G., Hofmann, A. W., & Class, C. (2012). How double volcanic chains sample geochemical anomalies from the lowermost mantle. *Earth and Planetary Science Letters*, *359-360*, 240–247. https://doi.org/10.1016/j.epsl.2012.09.057

French, S. W., & Romanowicz, B. (2015). Broad plumes rooted at the base of the Earth's mantle beneath major hotspots. *Nature*, *525*(7567), 95–99. https://doi.org/10.1038/nature14876

Fukao, Y., Widiyantoro, S., & Obayashi, M. (2001). Stagnant slabs in the upper and lower mantle transition region. *Reviews of Geophysics*, *39*(3), 291–323. https://doi.org/10.1029/1999RG000068

Gayer, E., Mukhopadhyay, S., & Meade, B. J. (2008). Spatial variability of erosion rates inferred from the frequency distribution of cosmogenic ^3He in olivines from Hawaiian river sediments. *Earth and Planetary Science Letters*, *266*(3-4), 303–315. https://doi.org/10.1016/j.epsl.2007.11.019

Graham, D. W. (2002). Noble gas isotope geochemistry of mid-ocean ridge and ocean island basalts: Characterization of mantle source reservoirs. *Reviews in Mineralogy and Geochemistry*, *4*, 247–317. https://doi.org/10.2138/rmg.2002.47.8

Graham, D. W., Castillo, P. R., Lupton, J. E., & Batiza, R. (1996). Correlated He and Sr isotope ratios in South Atlantic near-ridge seamounts and implications for mantle dynamics. *Earth and Planetary Science Letters*, *144*(3-4), 491–503. https://doi.org/10.1016/S0012-821X(96)00172-0

Graham, D. W., Hanan, B. B., Hémond, C., Blichert-Toft, J., & Albarède, F. (2014). Helium isotopic textures in Earth's upper mantle. *Geochemistry, Geophysics, Geosystems*, *15*, 2048–2074. https://doi.org/10.1002/2014GC005264

Graham, D. W., Jenkins, W., Schilling, J.-G., Thompson, G., Kurz, M. D., & Humphris, S. E. (1992). Helium isotope geochemistry of mid-ocean ridge basalts from the South Atlantic. *Earth and Planetary Science Letters*, *110*(1-4), 133–147. https://doi.org/10.1016/0012-821X(92)90044-V

Graham, D. W., Michael, P. J., & Shea, T. (2016). Extreme incompatibility of helium during mantle melting: Evidence from undegassed mid-ocean ridge basalts. *Earth and Planetary Science Letters*, *454*, 192–202. https://doi.org/10.1016/j.epsl.2016.09.016

Grand, S. P., van Der Hilst, R. D., & Widiyantoro, S. (1997). Global seismic tomography: A snapshot of convection in the Earth. *GSA Today*, *17*(7), 45–47. https://doi.org/10.1130/GSAT01707GW.1

Green, T. H. (1992). rocks from the Balleny Is, Antarctica. *Australian Journal of Earth Sciences*, *39*(5), 603–617. https://doi.org/10.1080/08120099208728053

Harðardóttir, S., Halldórsson, S. A., & Hilton, D. R. (2017). Spatial distribution of helium isotopes in Icelandic geothermal fluids and volcanic materials with implications for location, upwelling and evolution of the Icelandic mantle plume. *Chemical Geology*, *480*, 12–27. https://doi.org/10.1016/j.chemgeo.2017.05.012

Harpp, K. S., Hall, P. S., & Jackson, M. G. (2014). Galápagos and Easter: A tale of two hotspots. *Galapagos A Natural Laboratory for the Earth Sciences*, 27–40. https://doi.org/10.1002/9781118852538.ch3

Harrison, L. N., Weis, D., & Garcia, M. O. (2017). The link between Hawaiian mantle plume composition, magmatic flux, and deep mantle geodynamics. *Earth and Planetary Science Letters*, *463*, 298–309. https://doi.org/10.1016/j.epsl.2017.01.027

He, Y., & Wen, L. (2009). Structural features and shear-velocity structure of the "Pacific Anomaly". *Journal of Geophysical Research*, *114*, B02309. https://doi.org/10.1029/2008JB005814

Hilton, D. R., Grönvold, K., Macpherson, C. G., & Castillo, P. R. (1999). Extreme $^{3}He/^{4}He$ ratios in northwest Iceland: Constraining the common component in mantle plumes. *Earth and Planetary Science Letters*, *173*(1-2), 53–60. https://doi.org/10.1016/S0012-821X(99)00215-0

Hilton, D. R., MacPhersona, C. G., & Elliott, T. R. (2000). Helium isotope ratios in mafic phenocrysts and geothermal fluids from La Palma, the Canary Islands (Spain): Implications for HIMU mantle sources. *Geochimica et Cosmochimica Acta*, *64*(12), 2119–2132. https://doi.org/10.1016/S0016-7037(00)00358-6

Hoernle, K., Rohde, J., Hauff, F., Garbe-Schönberg, D., Homrighausen, S., Werner, R., & Morgan, J. P. (2015). How and when plume zonation appeared during the 132 Myr evolution of the Tristan Hotspot. *Nature Communications*, *6*(1), 7799. https://doi.org/10.1038/ncomms8799

Huang, S., Hall, P. S., & Jackson, M. G. (2011). Geochemical zoning of volcanic chains associated with Pacific hotspots. *Nature Geoscience*, *4*(12), 874–878. https://doi.org/10.1038/ngeo1263

Jackson, M. G., Becker, T. W., & Konter, J. G. (2018a). Evidence for a deep mantle source for EM and HIMU domains from integrated geochemical and geophysical constraints. *Earth and Planetary Science Letters*, *484*, 154–167. https://doi.org/10.1016/j.epsl.2017.11.052

Jackson, M. G., Becker, T. W., & Konter, J. G. (2018b). Geochemistry and distribution of recycled domains in the mantle inferred from Nd and Pb isotopes in oceanic hotspots: Implications for storage in the large low shear wave velocity provinces. *Geochemistry, Geophysics, Geosystems*, *19*, 3496–3519. https://doi.org/10.1029/2018GC007552

Jackson, M. G., Hart, S. R., Saal, A. E., Shimizu, N., Kurz, M. D., Blusztajn, J. S., & Skovgaard, A. C. (2008). Globally elevated titanium, tantalum, and niobium (TITAN) in ocean island basalts with high $^{3}He/^{4}He$. *Geochemistry, Geophysics, Geosystems*, *9*, Q04027. https://doi.org/10.1029/2007GC001876

Jackson, M. G., Konter, J. G., & Becker, T. W. (2017). Primordial helium entrained by the hottest mantle plumes. *Nature*, *542*(7641), 340–343. https://doi.org/10.1038/nature21023

Jackson, M. G., Kurz, M. D., & Hart, S. R. (2009). Helium and neon isotopes in phenocrysts from Samoan lavas: Evidence for heterogeneity in the terrestrial high $^{3}He/^{4}He$ mantle. *Earth and Planetary Science Letters*, *287*(3-4), 519–528. https://doi.org/10.1016/j.epsl.2009.08.039

Jephcoat, A. P. (1998). Rare-gas solids in the Earth's deep interior. *Nature*, *393*(6683), 355–358. https://doi.org/10.1038/30712

Kawabata, H., Hanyu, T., Chang, Q., Kimura, J. I., Nichols, A. R. L., & Tatsumi, Y. (2011). The petrology and geochemistry of St. Helena alkali basalts: Evaluation of the oceanic crust-recycling model for HIMU OIB. *Journal of Petrology*, *52*(4), 791–838. https://doi.org/10.1093/petrology/egr003

Kellogg, L. H., Hager, B. H., & van Der Hilst, R. D. (1999). Compositional stratification in the deep mantle. *Science*, *283*, 1881–1884.

King, S. D., & Adam, C. (2014). Hotspot swells revisited. *Physics of the Earth and Planetary Interiors*, *235*, 66–83. https://doi.org/10.1016/j.pepi.2014.07.006

Koelemeijer, P., Deuss, A., & Ritsema, J. (2017). Density structure of Earth's lowermost mantle from Stoneley mode splitting observations. *Nature Communications*, *8*(1), 1–10. https://doi.org/10.1038/ncomms15241

Konrad, K., Koppers, A. A. P., Steinberger, B., Finlayson, V. A., Konter, J. G., & Jackson, M. G. (2018). On the relative motions of long-lived Pacific mantle plumes. *Nature Communications*, *9*, 854. https://doi.org/10.1038/s41467-018-03277-x

Kruijer, T. S., & Kleine, T. (2018). No ^{182}W excess in the Ontong Java Plateau source. *Chemical Geology*, *485*, 24–31. https://doi.org/10.1016/j.chemgeo.2018.03.024

Kurz, M. D., 1982. *Helium isotope geochemistry of oceanic volcanic rocks: Implications for mantle heterogeneity and degassing*. Diss. Massachusetts Institute of Technology and Woods Hole Oceanographic Institution.

Kurz, M. D., Curtice, J., Fornari, D., Geist, D., & Moreira, M. (2009). Primitive neon from the center of the Galapagos hotspot. *Earth and Planetary Science Letters*, *286*(1-2), 23–34. https://doi.org/10.1016/j.epsl.2009.06.008

Kurz, M. D., & Geist, D. (1999). Dynamics of the Galapagos hotspot from helium isotope geochemistry. *Geochimica et Cosmochimica Acta*, *63*(23-24), 4139–4156. https://doi.org/10.1016/S0016-7037(99)00314-2

Kurz, M. D., Jenkins, W. J., Hart, S. R., & Clague, D. (1983). Helium isotopic variations in volcanic rocks from Loihi Seamount and the Island of Hawaii. *Earth and Planetary Science Letters*, *66*, 388–406. https://doi.org/10.1016/0012-821X(83)90154-1

Lanyon, R., Varne, R., & Crawford, A. J. (1993). Tasmanian Tertiary basalts, the Balleny plume, and opening of the Tasman Sea (southwest Pacific Ocean). *Geology*, *21*(6), 555–558. https://doi.org/10.1130/0091-7613(1993)021<0555:TTBTBP>2.3.CO;2

Lau, H. C. P., Mitrovica, J. X., Davis, J. L., Tromp, J., Yang, H.-Y., & Al-Attar, D. (2017). Tidal tomography constrains Earth's deep-mantle buoyancy. *Nature*, *551*, 321–326. https://doi.org/10.1038/nature24452

le Roex, A. P., Chevallier, L., Verwoerd, W. J., & Barends, R. (2012). Petrology and geochemistry of Marion and Prince Edward Islands, Southern Ocean: Magma chamber processes and source region characteristics. *Journal of Volcanology and Geothermal Research*, *223-224*, 11–28. https://doi.org/10.1016/j.jvolgeores.2012.01.009

Li, M., McNamara, A. K., & Garnero, E. J. (2014). Chemical complexity of hotspots caused by cycling oceanic crust through mantle reservoirs. *Nature Geoscience*, *7*(5), 366–370. https://doi.org/10.1038/ngeo2120

Li, M., McNamara, A. K., Garnero, E. J., & Yu, S. (2017). Compositionally-distinct ultra-low velocity zones on Earth's core-mantle boundary. *Nature Communications*, *8*(1), 177. https://doi.org/10.1038/s41467-017-00219-x

Lithgow-Bertelloni, C., & Richards, M. A. (1998). The dynamics of Cenozoic and Mesozoic plate motions. *Reviews of Geophysics*, *36*(1), 27–78. https://doi.org/10.1029/97RG02282

Lupton, J. E., Graham, D. W., Delaney, J. R., & Johnson, H. P. (1993). Helium isotope variations in Juan-De-Fuca Ridge basalts. *Geophysical Research Letters*, *20*(17), 1851–1854. https://doi.org/10.1029/93GL01271

Manga, M. (1996). Mixing of heterogeneities in the mantle: Effect of viscosity differences. *Geophysical Research Letters*, *23*(4), 403–406. https://doi.org/10.1029/96GL00242

Masters, G., Laske, G., & Gilbert, F. (2000). Matrix autoregressive analysis of free-oscillation coupling and splitting. *Geophysical Journal International*, *143*, 478–489. https://doi.org/10.1046/j.1365-246X.2000.01261.x

Montelli, R., Nolet, G., Dahlen, F. A., & Masters, G. (2006). A catalogue of deep mantle plumes: New results from finite-frequency tomography. *Geochemistry, Geophysics, Geosystems*, *7*, Q11007. https://doi.org/10.1029/2006GC001248

Moreira, M. (2013). Noble gas constraints on the origin and evolution of Earth's volatiles. *Geochemical Perspectives*, *2*(2), 229–403. https://doi.org/10.7185/geochempersp.2.2

Mukhopadhyay, S. (2012). Early differentiation and volatile accretion recorded in deep-mantle neon and xenon. *Nature*, *486*(7401), 101–104. https://doi.org/10.1038/nature11141

Mundl, A., Touboul, M., Jackson, M. G., Day, J. M. D., Kurz, M. D., Lekic, V., et al. (2017). Tungsten-182 heterogeneity in modern ocean island basalts. *Science*, *356*, 66–69. https://doi.org/10.1126/science.aal4179

Nelson, P. L., & Grand, S. P. (2018). Lower-mantle plume beneath the Yellowstone hotspot revealed by core waves. *Nature Geoscience*, *11*(4), 280–284. https://doi.org/10.1038/s41561-018-0075-y

Ni, S., Tan, E., Gurnis, M., & Helmberger, D. V. (2002). Sharp sides to the African superplume. *Science*, *296*, 1850–1852. https://doi.org/10.1126/science.1070698

Parai, R., Mukhopadhyay, S., & Lassiter, J. C. (2009). New constraints on the HIMU mantle from neon and helium isotopic compositions of basalts from the Cook-Austral Islands. *Earth and Planetary Science Letters*, *277*(1-2), 253–261. https://doi.org/10.1016/j.epsl.2008.10.014

Parmelee, D. E. F., Kyle, P. R., Kurz, M. D., Marrero, S. M., & Phillips, F. M. (2015). A new Holocene eruptive history of Erebus volcano, Antarctica using cosmogenic ^{3}He and ^{36}Cl exposure ages. *Quaternary Geochronology*, *30*, 114–131. https://doi.org/10.1016/j.quageo.2015.09.001

Payne, J. A., Jackson, M. G., & Hall, P. S. (2013). Parallel volcano trends and geochemical asymmetry of the Society Islands hotspot track. *Geology*, *41*(1), 19–22. https://doi.org/10.1130/G33273.1

Péron, S., Moreira, M., Colin, A., Arbaret, L., Putlitz, B., & Kurz, M. D. (2016). Neon isotopic composition of the mantle constrained by single vesicle analyses. *Earth and Planetary Science Letters*, *449*, 145–154. https://doi.org/10.1016/j.epsl.2016.05.052

Péron, S., Moreira, M., Putlitz, B., & Kurz, M. D. (2017). Solar wind implantation supplied light volatiles during the frst stage of Earth accretion. *Geochemical Perspectives Letters*, *3*, 151–159. https://doi.org/10.7185/geochemlet.1718

Pető, M. K., Mukhopadhyay, S., & Kelley, K. A. (2013). Heterogeneities from the first 100 million years recorded in deep mantle noble gases from the Northern Lau Back-arc Basin. *Earth and Planetary Science Letters*, *369-370*, 13–23. https://doi.org/10.1016/j.epsl.2013.02.012

Porcelli, D., & Halliday, A. N. (2001). The core as a possible source of mantle helium. *Earth and Planetary Science Letters*, *192*, 45–56. https://doi.org/10.1016/S0012-821X(01)00418-6

Rickers, F., Fichtner, A., & Trampert, J. (2013). The Iceland-Jan Mayen plume system and its impact on mantle dynamics in the North Atlantic region: Evidence from full-waveform inversion. *Earth and Planetary Science Letters*, *367*, 39–51. https://doi.org/10.1016/j.epsl.2013.02.022

Ritsema, J., Deuss, A., Van Heijst, H. J., & Woodhouse, J. H. (2011). S40RTS: a degree-40 shear-velocity model for the mantle from new Rayleigh wave dispersion, teleseismic traveltime and normal-mode splitting function measurements. *Geophysical Journal International*, *184*, 1223–1236. https://doi.org/10.1111/j.1365-246X.2010.04884.x

Rizo, H., Andrault, D., Bennett, N. R., Humayun, M., Brandon, A., Vlastelic, I., et al. (2019). 182W evidence for core-mantle interaction in the source of mantle plumes. *Geochemical Perspectives Letters*, *11*, 6–11. https://doi.org/10.7185/geochemlet.1917

Rizo, H., Walker, R. J., Carlson, R. W., Horan, M. F., Mukhopadhyay, S., Manthos, V., et al. (2016). Preservation of Earth-forming events in the tungsten isotopic composition of modern flood basalts. *Science*, *352*, 809–812. https://doi.org/10.1126/science.aad8563

Romanowicz, B. (2017). Geophysics: The buoyancy of Earth's deep mantle. *Nature*, *551*(7680), 308–309. https://doi.org/10.1038/551308a

Seton, M., Müller, R. D., Zahirovic, S., Gaina, C., Torsvik, T., Shephard, G., et al. (2012). Global continental and ocean basin reconstructions since 200 Ma. *Earth-Science Reviews*, *113*(3-4), 212–270. https://doi.org/10.1016/j.earscirev.2012.03.002

Simmons, N. A., Forte, A. M., Boschi, L., & Grand, S. P. (2010). GyPSuM: A joint tomographic model of mantle density and seismic wave speeds. *Journal of Geophysical Research*, *115*, B12310. https://doi.org/10.1029/2010JB007631

Starkey, N. A., Stuart, F. M., Ellam, R. M., Fitton, J. G., Basu, S., & Larsen, L. M. (2009). Helium isotopes in early Iceland plume picrites: Constraints on the composition of high ^{3}He/^{4}He mantle. *Earth and Planetary Science Letters*, *277*(1-2), 91–100. https://doi.org/10.1016/j.epsl.2008.10.007

Steinberger, B. (2000). Plumes in a convecting mantle: Models and observations for individual hotspots. *Journal of Geophysical Research*, *105*(B5), 11127–11152. https://doi.org/10.1029/1999JB900398

Steinberger, B., & Antretter, M. (2006). Conduit diameter and buoyant rising speed of mantle plumes: Implications for the motion of hotspots and shape of plume conduits. *Geochemistry, Geophysics, Geosystems*, *7*, Q11018. https://doi.org/10.1029/2006GC001409

Steinberger, B., & O'Connell, R. J. (1998). Advection of plumes in mantle flow: implications for hotspot motion, mantle viscosity and plume distribution. *Geophysical Journal International*, *132*(2), 412–434. https://doi.org/10.1046/j.1365-246x.1998.00447.x

Steinberger, B., Sutherland, R., & O'Connell, R. J. (2004). Prediction of Emperor-Hawaii seamount locations from a revised model of global plate motion and mantle flow. *Nature*, *430*, 167–173. https://doi.org/10.1038/nature02660

Stuart, F. M., Lass-Evans, S., Godfrey Fitton, J., & Ellam, R. M. (2003). High 3He/4He ratios in picritic basalts from Baffin Island and the role of a mixed reservoir in mantle plumes. *Nature*, *424*(6944), 57–59. https://doi.org/10.1038/nature01711

Su, W., & Dziewonski, A. M. (1997). Simultaneous inversion for 3-D variations in shear and bulk velocity in the mantle. *Physics of the Earth and Planetary Interiors*, *100*, 135–156. https://doi.org/10.1016/S0031-9201(96)03236-0

Tackley, P. J. (2000). Mantle convection and plate tectonics: Toward an integrated physical and chemical theory. *Science*, *288*, 2002–2007. https://doi.org/10.1126/science.288.5473.2002

Tackley, P. J. (2011). Living dead slabs in 3-D: The dynamics of compositionally-stratified slabs entering a "slab graveyard" above the core-mantle boundary. *Physics of the Earth and Planetary Interiors*, *188*(3-4), 150–162. https://doi.org/10.1016/j.pepi.2011.04.013

Tan, E., & Gurnis, M. (2005). Metastable superplumes and mantle compressibility. *Geophysical Research Letters*, *32*, L20307. https://doi.org/10.1029/2005GL024190

Thorne, M. S., Garnero, E. J., Jahnke, G., Igel, H., & Mcnamara, A. K. (2013). Mega ultra low velocity zone and mantle flow. *Earth and Planetary Science Letters*, *364*, 59–67. https://doi.org/10.1016/j.epsl.2012.12.034

To, A., Romanowicz, B., Capdeville, Y., & Takeuchi, N. (2005). 3D effects of sharp boundaries at the borders of the African and Pacific superplumes: Observation and modeling. *Earth and Planetary Science Letters*, *233*(1-2), 137–153. https://doi.org/10.1016/j.epsl.2005.01.037

Touboul, M., Kleine, T., Bourdon, B., Palme, H., & Wieler, R. (2007). Late formation and prolonged differentiation of the Moon inferred from W isotopes in lunar metals. *Nature*, *450*(7173), 1206–1209. https://doi.org/10.1038/nature06428
Tucker, J. M., & Mukhopadhyay, S. (2014). Evidence for multiple magma ocean outgassing and atmospheric loss episodes from mantle noble gases. *Earth and Planetary Science Letters*, *393*, 254–265. https://doi.org/10.1016/j.epsl.2014.02.050
Valbracht, P. J., Staudacher, T., Malahoff, A., & Allègre, C.-J. (1997). Noble gas systematics of deep rift zone glasses from Loihi Seamount, Hawaii. *Earth and Planetary Science Letters*, *150*(3-4), 399–411. https://doi.org/10.1016/S0012-821X(97)00094-0
Van Der Hilst, R. D., & Karason, H. (1999). Compositional heterogeneity in the bottom 1000 kilometers of Earth's mantle: Toward a hybrid convection model. *Science*, *283*, 1885–1888.
Van Der Hilst, R. D., Widiyantorot, S., & Engdahl, E. R. (1997). Evidence for deep mantle circulation from global tomography. *Nature*, *386*(6625), 578–584. https://doi.org/10.1038/386578a0
Wang, Y., & Wen, L. (2007). Geometry and P and S velocity structure of the "African Anomaly". *Journal of Geophysical Research*, *112*, B05313. https://doi.org/10.1029/2006JB004483
Weis, D., Garcia, M. O., Rhodes, J. M., Jellinek, M. A., & Scoates, J. S. (2011). Role of the deep mantle in generating the compositional asymmetry of the Hawaiian mantle plume. *Nature Geoscience*, *4*(12), 831–838. https://doi.org/10.1038/ngeo1328
Willbold, M., & Stracke, A. (2006). Trace element composition of mantle end-members: Implications for recycling of oceanic and upper and lower continental crust. *Geochemistry, Geophysics, Geosystems*, *7*, Q04004. https://doi.org/10.1029/2005GC001005
Willbold, M., & Stracke, A. (2010). Formation of enriched mantle components by recycling of upper and lower continental crust. *Chemical Geology*, *276*(3-4), 188–197. https://doi.org/10.1016/j.chemgeo.2010.06.005
Wolfe, C. J., Solomon, S. C., Laske, G., Collins, J. A., Detrick, R. S., Orcutt, J. A., et al. (2009). Mantle shear-wave velocity structure beneath the Hawaiian hot spot. *Science*, *326*, 1388–1390. https://doi.org/10.1126/science.1180165
Woodhouse, J. H., & Dziewonski, A. M. (1989). Seismic modelling of the Earth's large-scale three-dimensional structure. *Philosophical Transactions of the Royal Society of London. Series A*, *328*, 291–308.
Yuan, K., & Romanowicz, B. (2017). Seismic evidence for partial melting at the root of major hot spot plumes. *Science*, *357*, 393–397. https://doi.org/10.1126/science.aan0760
Zhong, S., McNamara, A., Tan, E., Moresi, L., & Gurnis, M. (2008). A benchmark study on mantle convection in a 3-D spherical shell using CitcomS. *Geochemistry, Geophysics, Geosystems*, *9*, Q10017. https://doi.org/10.1029/2008GC002048
Zhong, S., Zuber, M. T., Moresi, L., & Gurnis, M. (2000). Role of temperature-dependent viscosity and surface plates in spherical shell models of mantle convection. *Journal of Geophysical Research*, *105*(B5), 11063–11082. https://doi.org/10.1029/2000JB900003

References From the Supporting Information

Bräuer, K., Kämpf, H., Niedermann, S., & Strauch, G. (2013). Indications for the existence of different magmatic reservoirs beneath the Eifel area (Germany): A multi-isotope (C, N, He, Ne, Ar) approach. *Chemical Geology*, *356*, 193–208. https://doi.org/10.1016/j.chemgeo.2013.08.013
Camp, V. E., & Hanan, B. B. (2008). A plume-triggered delamination origin for the Columbia River Basalt Group. *Geosphere*, *4*(3), 480. https://doi.org/10.1130/GES00175.1
Caracausi, A., Avice, G., Burnard, P. G., Füri, E., & Marty, B. (2016). Chondritic xenon in the Earth's mantle. *Nature*, *533*(7601), 82–85. https://doi.org/10.1038/nature17434
Clarke, W. B., Jenkins, W. J., & Top, Z. (1976). Determination of tritium by mass spectrometric measurement of ^{3}He. *International Journal of Applied Radiation and Isotopes*, *27*(9), 515–522. https://doi.org/10.1016/0020-708X(76)90082-X
Graham, D. W., Lupton, J. E., Albarède, F., & Condomines, M. (1990). Extreme temporal homogeneity of helium isotoeps at Piton de la Fournaise, Reunion Island. *Nature*, *347*(6293), 545–548. https://doi.org/10.1038/347545a0
Graham, D. W., Michael, P. J., & Shea, T. (2016). Extreme incompatibility of helium during mantle melting: Evidence from undegassed mid-ocean ridge basalts. *Earth and Planetary Science Letters*, *454*, 192–202. https://doi.org/10.1016/j.epsl.2016.09.016
Hanyu, T., Dunai, T. J., Davies, G. R., Kaneoka, I., Nohda, S., & Uto, K. (2001). Noble gas study of the Reunion hotspot: Evidence for distinct less-degassed mantle sources. *Earth and Planetary Science Letters*, *193*(1-2), 83–98. https://doi.org/10.1016/S0012-821X(01)00489-7
Kincaid, C., Druken, K. A., Griffiths, R. W., & Stegman, D. R. (2013). Bifurcation of the Yellowstone plume driven by subduction-induced mantle flow. *Nature Geoscience*, *6*(5), 395–399. https://doi.org/10.1038/ngeo1774
Liu, L., & Stegman, D. R. (2012). Origin of Columbia River flood basalt controlled by propagating rupture of the Farallon slab. *Nature*, *482*(7385), 386–389. https://doi.org/10.1038/nature10749
Mamyrin, B. A. (1970). Determination of the isotopic composition of atmospheric helium. *Geochemistry International*, *7*, 498–505.
Sleep, N. H., Ebinger, C. J., & Kendall, J.-M. (2002). Deflection of mantle plume material by cratonic keels. *Geological Society London Special Publications*, *199*(1), 135–150. https://doi.org/10.1144/GSL.SP.2002.199.01.08
Smith, R. B., Jordan, M., Steinberger, B., Puskas, C. M., Farrell, J., Waite, G. P., et al. (2009). Geodynamics of the Yellowstone hotspot and mantle plume: Seismic and GPS imaging, kinematics, and mantle flow. *Journal of Volcanology and Geothermal Research*, *188*(1-3), 26–56. https://doi.org/10.1016/j.jvolgeores.2009.08.020
Staudacher, T., Sarda, P., & Allegre, C. J. (1990). Noble gas systematics of Reunion Island, Indian Ocean. *Chemical Geology*, *89*(1-2), 1–17. https://doi.org/10.1016/0009-2541(90)90057-E
Trieloff, M., Kunz, J., & Allègre, C. J. (2002). Noble gas systematics of the Réunion mantle plume source and the origin of primordial noble gases in Earth's mantle. *Earth Planet. Sci. Lett.*, *200*(3-4), 297–313. https://doi.org/10.1016/S0012-821X(02)00639-8